The Capacitance of Nickel Pattern Electrodes on Zirconia Electrolyte

M. C. Doppler,[a,b] J. Fleig,[b,*] M. Bram,[a,c] and A. K. Opitz[a,b,z]

[a] *Christian Doppler Laboratory for Interfaces in Metal-Supported Electrochemical Energy Converters, 1060 Wien, Austria*
[b] *Institute of Chemical Technologies and Analytics, TU Wien, 1060 Vienna, Austria*
[c] *Forschungszentrum Jülich GmbH, Institute of Energy and Climate Research, Materials Synthesis and Processing (IEK-1), 52425 Jülich, Germany*

Micro-structured thin-film electrodes were employed to investigate the capacitive behavior of nickel on yttria-stabilized zirconia (YSZ) electrolytes by means of electrochemical impedance spectroscopy. Electrodes with different shapes and electrode areas clearly showed a linear relationship between capacitance and the electrode area. Electrostatic double layer models, however, could not explain the observed area specific capacitance value of ca. 3 F/m^2. This fact, the characteristic voltage dependence with a hysteresis, and the effect of H_2S on the electrode capacitance indicate substantial contributions of a chemical capacitance. Possible types of chemical capacitance in the system Ni(H_2/H_2O)/YSZ are discussed and an oxygen partial pressure dependent mechanism change is suggested.
 [DOI: 10.1149/2.0951610jes] All rights reserved.

Manuscript submitted May 13, 2016; revised manuscript received July 18, 2016. Published August 25, 2016.

Solid oxide fuel cells (SOFCs) present a promising technology for direct conversion of chemical energy into electrical energy due to their high efficiency and fuel flexibility while causing little polluting emissions.[1] Much research effort was devoted to the optimization of SOFC cathodes and cathodic polarization losses were substantially reduced.[2] Consequently, in modern SOFCs the anode, which usually consists of a nickel/yttria stabilized zirconia (YSZ) cermet, may (again) contribute significantly to the overall cell losses. However, despite many investigations of the electrochemical anode behavior,[3–30] fundamental properties of Ni/YSZ anodes are still far from being well understood. Therefore, considerable research still needs to be done to gain an in-depth understanding of the electrochemistry of Ni/YSZ electrodes, and to further optimize the performance of SOFC anodes.

While having advantageous properties for application in operating SOFCs, Ni/YSZ cermet electrodes are often only of limited use for such fundamental research studies, since transport resistances due to ion conduction or gas diffusion and ill-defined geometry make data analysis very challenging. In contrast, model electrodes and in particular micro-structured thin-film electrodes – often referred to as pattern electrodes – are particularly suited for basic research studies.[9–30] One of the main advantages of pattern electrodes is that their geometry can be controlled in a well-defined manner and thus geometry dependencies of electrochemical parameters can be obtained much easier compared to cermet electrodes.[31,32]

So far, most research effort has been put into explaining the resistive behavior of Ni/YSZ model electrodes, while capacitive effects are still much less understood, despite their importance in impedance measurements. In previous literature high area specific capacitance (ASC) values of Ni/YSZ electrodes were reported, which could not be explained by a classical Helmholtz-type double layer.[12,33,34] A comparison of Ni, Pt and Au electrodes on YSZ also showed significantly higher capacitances of the Ni electrodes, further suggesting additional contributions to capacitive effects.[12] Proposed mechanisms for the increased capacitance values were based on chemical processes at the electrode, such as proton ad/absorption[33] and valence changes of impurity ions.[34] Another capacitive model of metal electrodes on YSZ, based on a modified Gouy-Chapman theory, was developed by Hendriks and coworkers.[35] In their study on blocking Au/YSZ electrodes in nitrogen they showed that the observed ASC dependency on both the applied bias and the oxygen vacancy concentration are in reasonable agreement with their model.

In this contribution, patterned Ni electrodes of different shape and size were used to further investigate the capacitive behavior of Ni on YSZ electrolytes. Dependencies on area, electrode shape, bias voltage, temperature, oxygen partial pressure and H_2S exposure were measured. The latter experiments may give further information on the highly relevant topic of sulfur poisoning when operating SOFCs with S-containing fuels. Absolute values of ASC as well as voltage dependencies of capacitances are compared to available models and contributions of chemical capacitances are discussed.

Experimental

A porous counter electrode was prepared by screen printing of NiO/YSZ paste on the unpolished (bottom) side of a one-side polished 0.5 mm thick (111) YSZ single crystals (9.5 mol% Y_2O_3, Crystec, GER) and fired at 1250°C for 2 h in air. A 1200 nm thick Ni film was deposited on the polished (top) side via magnetron sputtering (99.99% Ni target, Advent RM, UK). The film was subsequently recrystallized at 750°C for 4 h in an atmosphere containing 2.5% H_2/0.15% H_2O/balance Ar. Micro-structuring of the film was done via photolithography. The sample was spincoated with ma-N 1420 Negativ Photoresist (Micro Resist Technology GmbH, GER) for 30 s at 150 Hz, baked for 2 min at 100°C, exposed to UV radiation for 40 s (350 W high pressure Hg lamp, Ushio Inc., JAP), developed with ma-D 533S Developer for Photoresist (Micro Resist Technology GmbH, GER) and finally etched in aqua regia. This led to differently shaped Ni anodes with nominal circumferences (triple phase boundary lengths) of 2.5 mm and nominal areas ranging from 0.09 mm^2 to 0.5 mm^2. Sketches of the used electrode shapes and microscopic images of typical microelectrodes are shown in Figures 1a and 1b.

Electrodes covered with a YSZ layer were prepared by depositing a 30 nm thick YSZ film on top of the recrystallized Ni film using pulsed laser deposition. The background pressure was 0.04 mbar of ARCAL (2.5% H_2 in Ar) and the temperature during deposition was 650°C. Target ablation was performed using a KrF excimer laser (Coherent Lambda Physics, Germany) with a pulse frequency of 5 Hz and a nominal energy per puls of 400 mJ for 10 min. After structuring of the photoresist the YSZ layer was Ar-ion beam etched and the remaining Ni film was etched by aqua regia; thus two types of electrodes were investigated, see the sketch in Figure 1c.

Impedance measurements were performed in a quartz tube, where the patterned thin film electrode was contacted by Ni (or Pt, if noted as such) needles attached to a quartz glass cantilever. This contacting method was also utilized for covered electrodes. A detailed description of the equipment used for these measurements has been given elsewhere.[28] All microelectrodes were geometrically characterized by optical microscopy before the electrochemical measurements. Unless otherwise noted, experiments were performed at 800°C in an

*Electrochemical Society Member.
[z]E-mail: alexander.opitz@tuwien.ac.at

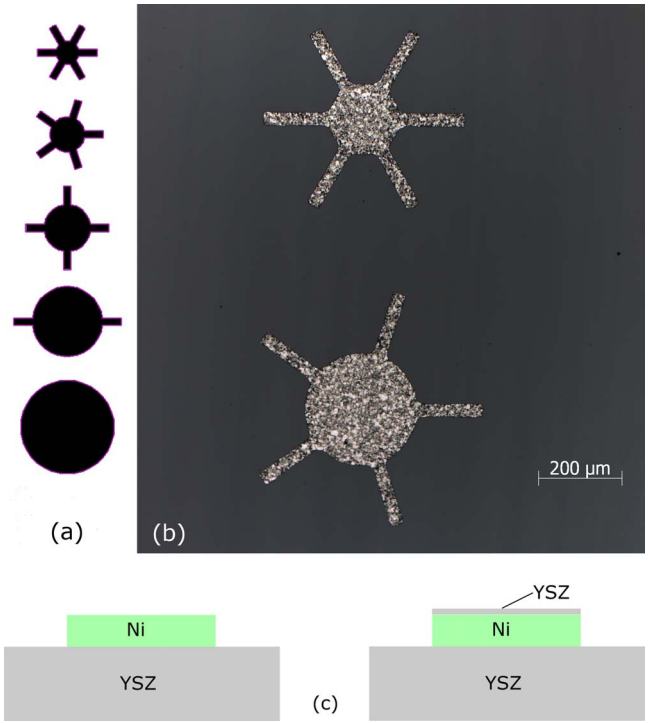

Figure 1. (a) Schematic drawing of electrode designs with equal circumference and varying area used in this study. (b) Bright field reflected light microscopic image of typical electrodes after measurement. (c) Schematic side-view of a sample without (lhs) and with a YSZ cover (rhs).

atmosphere consisting of 2.5% H_2/0.15% H_2O/balance Ar (if noted 10 ppm H_2S were added). Impedance measurements were done using a Novocontrol Alpha-A impedance analyzer with a POT/GAL interface (Novocontrol Technologies, GER). The AC stimulus was 10 mV (root-mean-square). The typical frequency range was 1 MHz to 5 mHz, but was adjusted if necessary. Temperature ramps for the experiments were set to 1°C/min to safely ensure a thermal equilibration of the samples at the measurement conditions.

The reader should note that the significance level for this study is defined as $\alpha = 0.05$, meaning that the null hypothesis from statistical tests is rejected when the respective p-value is below 0.05.

Results

Impedance spectra.—A typical impedance spectrum recorded under the aforementioned conditions is shown in Figure 2. The spectrum consists of a high frequency axis intercept (hardly visible in Figure 2) and one dominating arc in the medium to low frequency range. The latter exhibits the shape of a depressed and slightly asymmetric semicircle.

For data parameterization by a complex non-linear least squares (CNLS) fitting routine (software: Z-View, Scribner, USA) the simple equivalent circuit in Figure 2 was chosen. The series resistance R_spread is mainly caused by the spreading resistance of ion conduction in the YSZ electrolyte,[36] while the second resistance R_Pol is attributed to the electrode's polarization resistance. To account for the depression of the electrode arc a constant phase element (CPE) was used in the circuit instead of a capacitor. (Please note: Modeling the slight asymmetry of the electrode feature by an additional R/CPE element was not straightforwardly possible – this easily lead to over-parameterization and was thus omitted.) The impedance of a CPE element is defined as

$$Z_Q = {Q_0}^{-1}(i\omega)^{-n} \qquad [1]$$

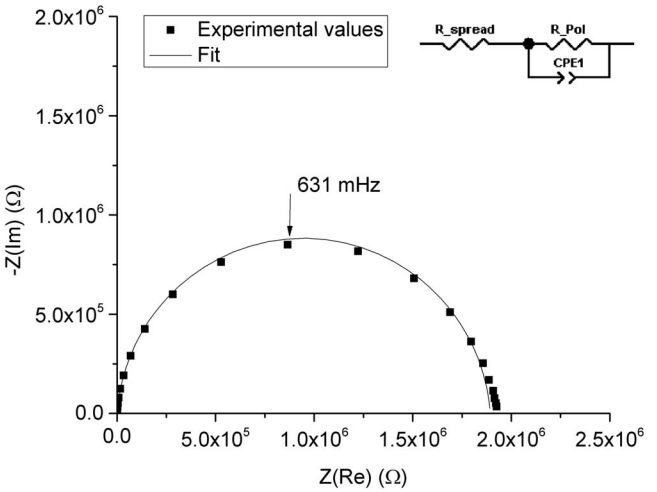

Figure 2. Nyquist plot of a typical impedance spectrum (symbols) and corresponding CNLS-fit (line). The equivalent circuit used for fitting is shown in the top right corner. Fit parameters: R_spread = 392 Ω, R_Pol = 1.89 MΩ, Q_0 = 1.56E-7 $Ss^{0.956}$, n = 0.956. Conditions: T = 800°C, 2.5% H_2/0.15% H_2O/balance Ar, Ni needle.

with Q_0 the admittance value at $\omega = 1\ s^{-1}$, i the imaginary unit, ω the angular frequency and n a number between -1 (ideal inductance) and 1 (ideal capacitance). In a CNLS fit Q_0 and n are usually used as fitting parameters. Since in this work values of n are between 0.88 and 0.96 and therefore sufficiently close to 1, the constant phase element can be interpreted in terms of a non-ideal capacitor. The corresponding capacitance can be calculated by the formula[37]

$$C = \left(R^{1-n}Q_0\right)^{1/n} \qquad [2]$$

with R being the resistance parallel to the CPE-element. Throughout this paper only capacitance values obtained by Eq. 2 will be discussed and referred to as electrode capacitance.

Electrode capacitance dependence on area.—In order to determine the geometry dependence of the electrode capacitance, electrodes of different area but equal triple phase boundary (TPB) lengths were electrochemically characterized. The shapes of these electrodes are different as shown in Figure 1a. For this measurement series the TPB length of the electrodes was evaluated as $l_{TPB} = 2.73 \pm 0.11$ mm. The scattering of l_{TPB} can be regarded as rather small compared to the variation of the area, which covered a range of 0.09 mm^2 to 0.5 mm^2. A plot of capacitance values as a function of electrode area for two different contacting needles is shown in Figure 3a and linear regression parameters are given in Table I. The graph indicates that for both Pt and Ni needles a linear relationship between capacitance and area holds true. Comparison of the slopes shows no significant difference between the two needles (t-test assuming equal variance; p = 0.15). For both an area-specific capacitances of about 3 F/m^2 is found. The 95% confidence interval for the C-intercept are $(-5.1 \pm 2.8) \cdot 10^{-8}$ F for the Ni needle and $(-6.6 \pm 2.0) \cdot 10^{-8}$ F for the Pt needle, respectively. The intercept is therefore indeed statistically significantly below 0. This negative intercept may originate from an electrode area that does not contribute to the capacitance; a likely candidate may be the area covered by the contacting needle. Another measurement series was performed on circular microelectrodes of different diameter at 750°C in 2.5% H_2/2% H_2O/balance Ar (Figure 3b). In this series, electrodes had the same shape but areas as well as TPB lengths varied. Essentially, the same results as for series 1 (Figure 3a) were found: a small intercept and a linear relation between capacitance and area. Hence, when neglecting the small axis intercept we can conclude from these measurements that the area specific electrode capacitance does neither depend on the size of the electrode nor on its shape.

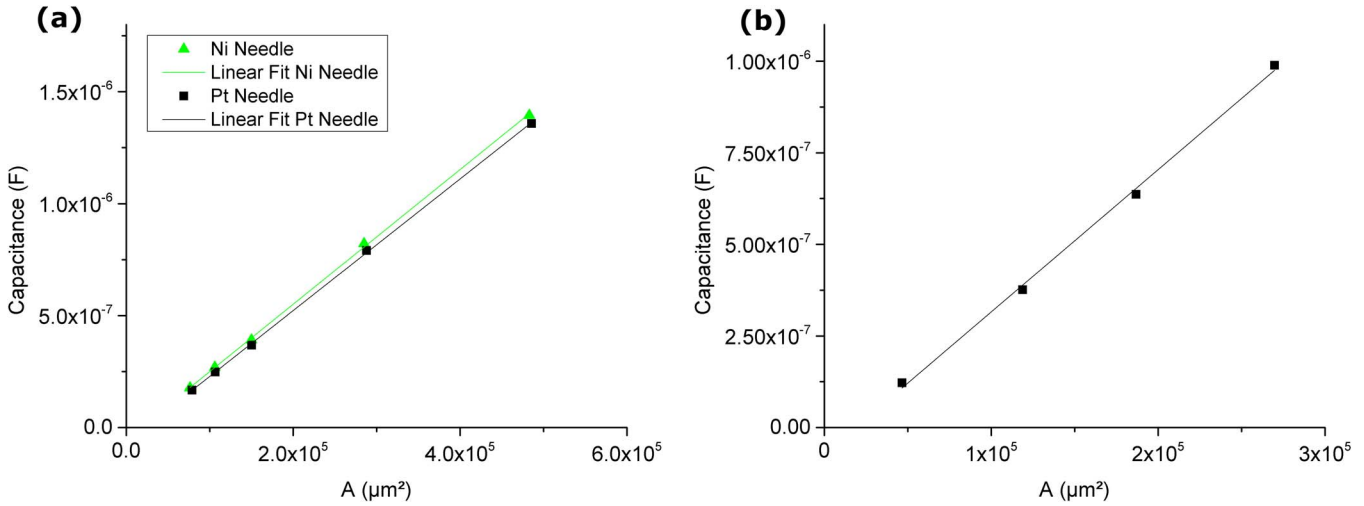

Figure 3. (a) Electrode capacitance values of electrodes with the same triple phase boundary length plotted as a function of the electrode area. Experimental points agree well with a linear fit with a negative capacitance-intercept. Conditions: T = 800°C, 2.5% H_2/0.15% H_2O/balance Ar. (b) Electrode capacitance values of circular electrodes with varying diameter plotted as a function of the electrode area. A linear fit agrees well with the data. Conditions: T = 750°C, 2.5% H_2/2% H_2O/balance Ar, Ni needle.

Table I. Linear fit results of area vs. electrode capacitance data. Fitting formula: C = k*A + d.

Description	d [µF]	Std.err. d [µF]	k [F/m^2]	Std. err. k [F/m^2]	R^2
Ni needle Figure 3a	−0.051	0.0087	3.01	0.033	0.99952
Pt needle Figure 3a	−0.066	0.0064	2.94	0.023	0.99973
Pre-S-exposure Figure 5	−0.04	0.024	2.99	0.086	0.99751
S-Exposed Figure 5	−0.045	0.0080	2.57	0.028	0.99964
YSZ cover Figure 6	−0.08	0.023	2.92	0.079	0.9978

Influence of H_2S.—A typical effect of hydrogen sulfide on the capacitance of Ni electrodes with and without YSZ cover at 800°C is shown in Figure 4. It can be seen that upon addition of 10 ppm H_2S to the feed gas the capacitance of all electrodes decreases within the experimental time resolution of ∼25 min. After removal of H_2S in the gas feed the capacitance quickly increases and eventually returns to values similar to pre-poisoning conditions. The plot in Figure 5 compares pristine and poisoned capacitance values for different electrode sizes of non-covered electrodes. The graph shows that capacitances under H_2S still follow a linear relationship with the area, but with a significantly lower slope (i.e. ASC) compared to the pre-poisoned values. Detailed results of the linear regressions are given in Table I. It should be noted that the measurement series "Ni needle Figure 3" and "Pre-S-exposure Figure 5" were measured under the same conditions on different samples and show very similar slopes. This difference in slope is not statistically significant (p = 0.82) which demonstrates the reproducibility of the measurements.

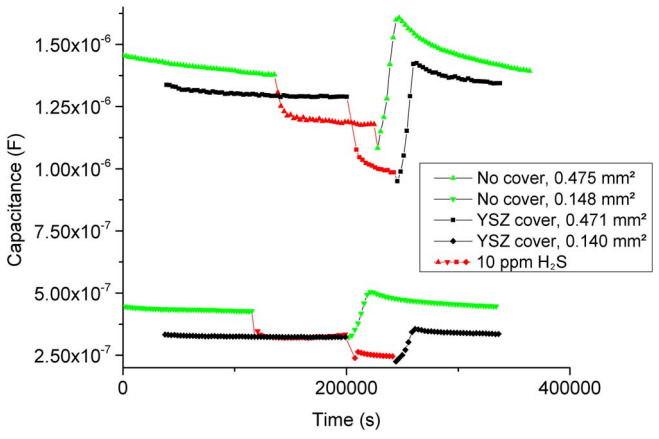

Figure 4. Capacitance of pristine electrodes and electrodes with YSZ covers as a function of time in a sulfur exposure experiment. Upon feeding 10 ppm H_2S into the gas feed (sulfur exposure is marked by red points) the capacitance drops quickly and again increases after removal of H_2S in the atmosphere. Conditions: T = 800°C, 2.5% H_2/0.15% H_2O/(10 ppm H_2S)/balance Ar, Ni needle.

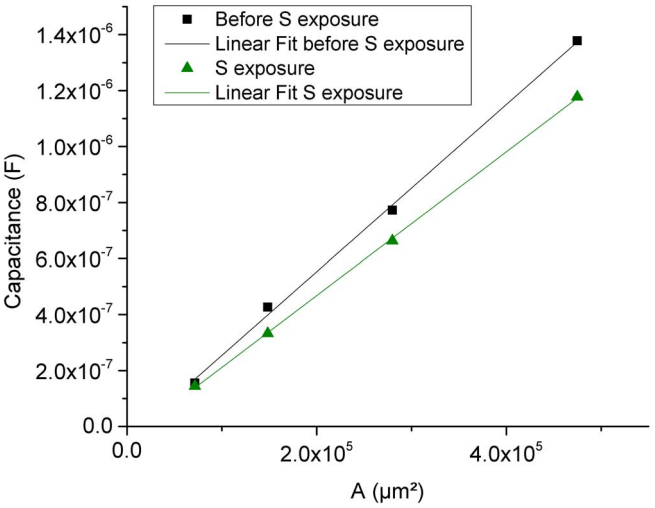

Figure 5. Electrode capacitance as a function of electrode area before and during sulfur exposure. The pre-exposure values are from the last measurement before exposure, the sulfur exposed values the last before H_2S removal from the gas feed. Conditions: T = 800°C, 2.5% H_2/0.15% H_2O/(10 ppm H_2S)/balance Ar, Ni needle.

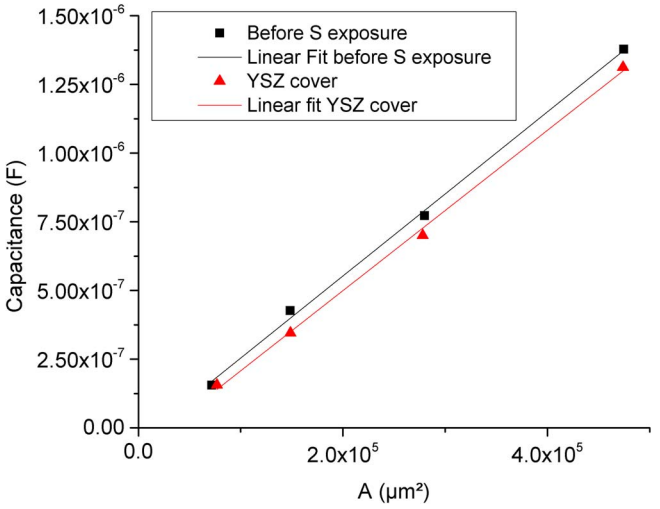

Figure 6. Comparison of capacitance values of electrodes with and without a YSZ cover on top of the Ni. Values for uncovered electrodes were taken from electrodes before sulfur poisoning (see Figure 5). Conditions: T = 800°C, 2.5% H_2/0.15% H_2O/balance Ar, Ni needle.

Covered Ni electrodes.—The effect of depositing 30 nm YSZ on top of Ni electrodes is shown in Figure 6 and linear regression details are summarized in Table I. It can be seen that the area specific capacitance for both measurements is very similar; the difference in slopes is not statistically significant ($p = 0.59$). Slightly different axis intercepts may reflect different needle contact areas. Also the effect of H_2S was not changed by the YSZ cover layer, see Fig. 4.

Influence of bias.—Impedance spectra for DC bias values ranging from −400 mV to +250 mV at various voltage steps were recorded for two water partial pressures with electrodes of different size. Besides small low-frequency inductive loops under high bias voltages (not included in the fit), the spectrum shape under bias voltage did not change compared to the unpolarized electrode. The resulting electrode capacitance was obtained by the fitting procedure discussed above and is plotted versus the bias voltage in Figure 7. Due to small counter electrode and electrolyte resistances the bias voltage is virtually identical to the overpotential at the Ni electrode. In the highly cathodic regime the capacitance increases strongly upon stronger polarization with little to no hysteresis, while in the other regime a moderately positive association between bias voltage and electrode capacitance with a kind of hysteresis can be found. This rather complex bias dependence is independent of the electrode size (Figure 7b, logarithmic plot), but turns out to be oxygen partial pressure dependent. Figure 7a shows that the curve shifts on the bias voltage axis for different water contents in the measurement atmosphere. For 2% water the minimum capacitance shifts −125 mV compared to the 0.15% water measurement. The voltage difference is thus in good agreement with the Nernst voltage between the atmospheres (−120 mV). This suggests that the transition between the two distinct capacitive regimes can be expressed in terms of an equilibrium oxygen partial pressure without additional bias voltage; a pressure of $7 \cdot 10^{-24}$ bar results. Differences in absolute electrode capacitance values are largely due to different electrode areas.

Influence of temperature.—Capacitance values obtained at different temperatures without bias voltage are shown in Figure 8. The figure shows a positive relation between the electrode capacitance and the temperature with a small hysteresis. The data correspond to a very small activation energy of 0.13 eV.

Structure of the Ni/YSZ interface.—A high resolution transmission electron microscope image of the Ni/YSZ interface is shown in Figure 9. Between the Ni and YSZ crystals a ∼1 nm thick interlayer can be found, which appears to be of oxidic nature. It has been reported for free YSZ surfaces[38–40] that such a layer could be the result of structural re-arrangement at the interface but might also include impurities such as Si segregated from YSZ.

Discussion

Electrostatic models.—The most well-known type of electrochemical double layer is the Helmholtz double layer. In this model the interface capacitance can be calculated as for a plate capacitor and, assuming $\varepsilon_r = 10$ and d = 250 pm (the diameter of an oxide ion), an ASC in the range of 0.35 F/m^2 would be expected. Since the experimental value of ∼3 F/m^2 is almost an order of magnitude higher than the expected value, it can be concluded that a Helmholtz double layer is not the (main) source of the observed electrode capacitance.

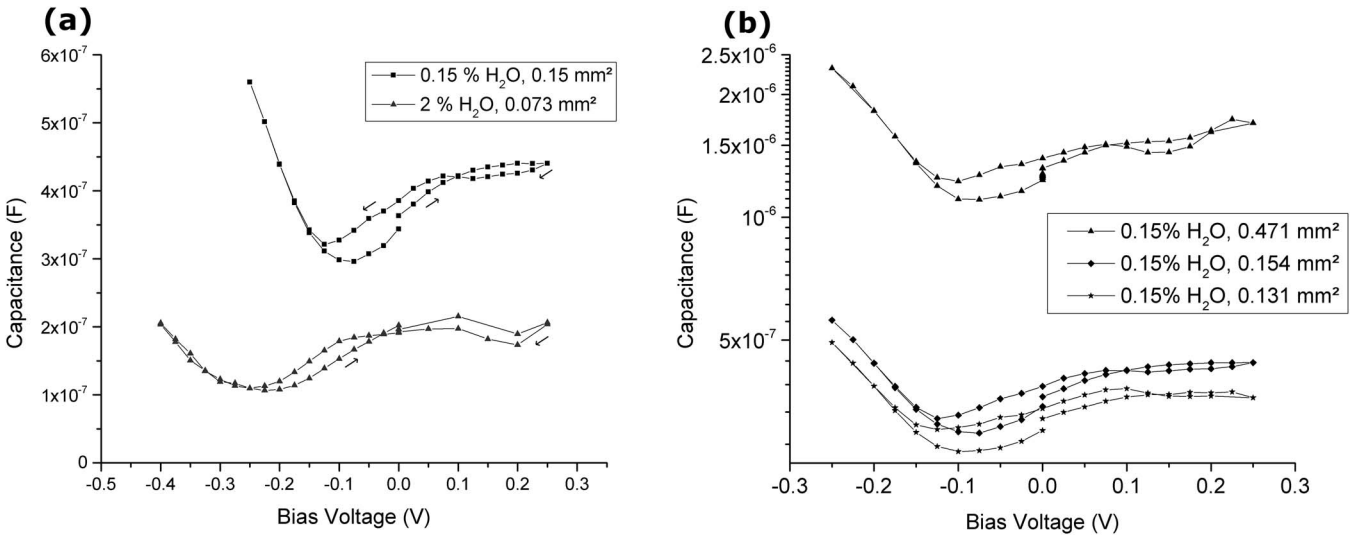

Figure 7. (a) Dependence of the electrode capacitance on the bias voltage of electrodes at 2 different water partial pressures. The electrode areas are 0.154 mm^2 (water content of 0.15%) and 0.073 mm^2 (water content of 2%). Conditions: T = 800°C, 2.5% H_2/var. % H_2O/balance Ar, Ni needle. (b) Dependence of the electrode capacitance on the bias voltage for electrodes with different area in the same atmosphere. Conditions: T = 800°C, 2.5% H_2/0.15% H_2O/balance Ar, Ni needle.

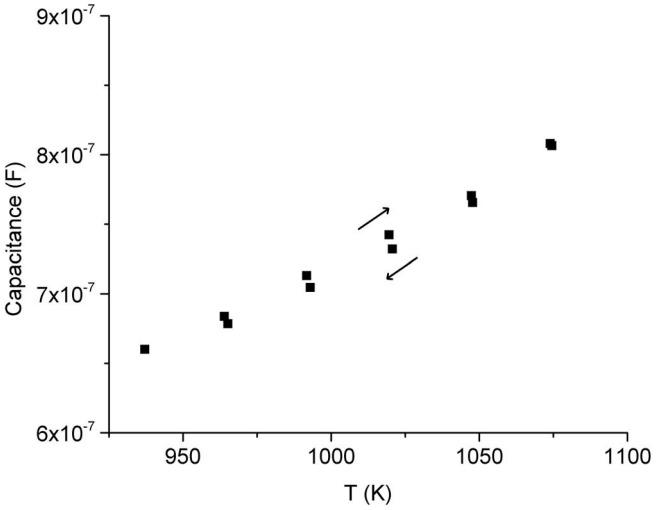

Figure 8. Temperature dependence of the electrode capacitance. The measurement was performed on an electrode with an area of 0.280 mm^2 by first decreasing and then increasing the temperature. Conditions: T = var.°C, 2.5% H_2/0.15% H_2O/balance Ar, Ni needle.

Similar conclusions have been reached in Refs. 33, 34 also assuming the 1 nm thin interfacial layer in Figure 9 to act as an insulating oxide can hardly explain the capacitance. Its relative permittivity would have to be ∼400 and thus far beyond values expected for typical interfacial phases (e.g. SiO_x).

As for diffuse double layer models ions cannot approach the metal surface closer than in the Helmholtz model, the upper limit of predicted capacitances of such models is again the capacitance of the Helmholtz model. This fact is also reflected in the Stern model.[41] The diffuse space charge layer model described by Hendriks et al.[35] is a modified Gouy-Chapman model with only one mobile species and oxygen vacancy concentration limitation. However, since it does not include metal approach limitation and interaction of oxygen vacancies its applicability is limited and not appropriate in our case.

Additionally, no effect of sulfur exposure on the capacitance is expected in electrostatic models and the complex dependence on the bias voltage is also not in accordance with simple models. It can therefore be concluded that neither a Helmholtz double layer nor a diffuse space charge layer is responsible for the observed capacitive behavior.

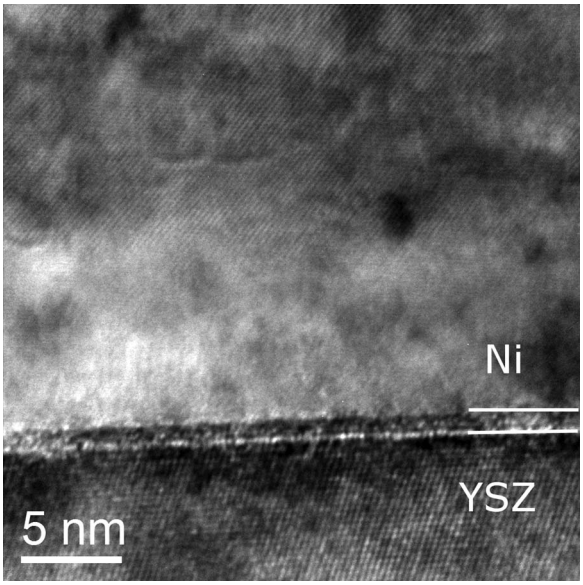

Figure 9. HR-TEM image of the Ni/YSZ interface.

Chemical capacitance models.—An alternative to the classical electrostatic capacitance models described above are capacitors based on faradaic processes with accumulation of reactants – often referred to as chemical capacitances. Since the measured capacitance scales linearly with the Ni electrode area this accumulation has to occur either at the Ni surface, or in the Ni bulk or at the interface between Ni and YSZ.

Since sulfur exposure does affect the electrode capacitance and is well-known in the SOFC community for adsorption on the Ni surface,[42] surface adsorbates as a reservoir of redox active species are firstly discussed as a possible explanation of the capacitive behavior. In this case, any substantial concentration change of adsorbed species would show a great impact on the capacitance. Modifying the surface of the Ni electrode by deposition of YSZ on top does not have a significant influence on the ASC. It can therefore be concluded that adsorbates on the Ni surface cannot explain the observed capacitive behavior. However, sulfur is also known to dissolve in Ni (under measurement conditions ∼40 ppm[43]) and then to segregate to the grain boundaries.[44] Hence, dissolved sulfur could also change concentrations of species in the bulk and/or at the Ni/YSZ interface and thereby affect the observed capacitance. One can assume that such a diffusion process of sulfur might take some time and causes a delay in the capacitance change after sulfur exposure. However, since our gas exchange and measurement time was in the range of 25 minutes, we may easily miss this time dependence. The instantaneous change seen in Figure 4 is thus possibly only an apparent one. The effect of sulfur on the ASC was not affected by a YSZ cover layer on the Ni electrode. This either means that diffusion of sulfur species through Ni is still possible due to some cracks in the YSZ cover layer or that the sulfur diffusion anyway takes place primarily along the YSZ/Ni interface. In the latter case, rather fast sulfur diffusion is required; this is conceivable since the fast sulfur surface diffusion on Ni was also reported in literature.[45]

In the following, five possible types of chemical capacitances are considered which either originate in the bulk (III) or at the Ni/YSZ interface (I, II, IV, V). Each mechanism is discussed not only in terms of its ability to explain the absolute ASC values, but also in the light of the bias dependency of the electrode capacitance since the bias effect exhibits two distinct regions – a linear region below an equilibrium oxygen partial pressure of $7 \cdot 10^{-24}$ bar without hysteresis and a region of weaker bias-dependency but with hysteresis above $7 \cdot 10^{-24}$ bar oxygen. This could indicate a switch in the dominant capacitive mechanism, which due to lacking discontinuities in the bias dependency graph is probably not caused by a phase change.

I) *Oxide non-stoichiometry:* The most common mechanism leading to chemical capacitances of mixed conducting SOFC cathodes is based on oxygen stoichiometry change. Even though nickel electrodes are not mixed oxide ion/electron conductors, a similar effect might take place for example in the interlayer at the Ni/YSZ boundary, particularly if an oxide with reducible ions is present. (For $Ni_{1-x}O$, however, mechanism IV, which is based on a phase formation rather than on a pure stoichiometry change, is regarded as more probable – see below). The chemical capacitance due to such an oxygen stoichiometry change can be estimated by

$$ASC = \frac{(ez_i)^2}{k_B T} c_i s \qquad [3]$$

where e is the elementary charge, z_i is the number of charges per charge carrier, k_B the Boltzmann constant, T the temperature, s the thickness of the corresponding layer and c_i the minority charge carrier concentration involved in the process, typically either oxygen vacancies or electrons or electron holes.[46] However, oxygen non-stoichiometry in the 1 nm thin layer of unknown composition, visible in HT-TEM, could only lead to such

a high capacitance if its electron concentration was larger than $10^{21}\ cm^{-3}$.

A strongly related option of a chemical capacitance is based on stoichiometry changes in YSZ. In air, contributions of YSZ to any chemical capacitance via oxide stoichiometric changes are negligible due to very low concentrations of electronic charge carriers. In hydrogen, however, electron concentrations in YSZ are enhanced and they further increase upon cathodic polarization. For a cathodic polarization of −250 mV in the measurement atmosphere with 0.15% water (equilibrium oxygen partial pressure of $p_{O_2} = 3.2 \cdot 10^{-26}\ bar$) a YSZ electron concentration of $[e] = 1.1 \cdot 10^{20}\ \mathrm{cm}^{-3}$ can be estimated.[47] According to Equation 3 the measured ASC would thus require stoichiometry changes in a YSZ layer with a thickness of only ∼15 nm assuming constant electrochemical potentials in this region. A further analysis including the exact potential distribution in the YSZ is beyond the scope of this study. Yet this estimate shows that such a mechanism is plausible, at least for the negative voltages without capacitance hysteresis. It would also be in qualitative agreement with the increase of the capacitance for higher cathodic voltages.

II) *Interface impurities:* A mechanism involving valence changes of impurities segregated to the Ni/YSZ interface was suggested by Hansen et al.[34] In their study, point electrodes, which are Ni wires pressed onto a YSZ substrate, were used. This approach led to significant impurity segregation, which even resulted in impurity ridges. Yet the thin-film electrodes used in our study exhibit a much more favorable surface-to-volume ratio and were prepared from highly pure Ni; the effect of impurity segregation, if there is any, should therefore be greatly reduced. While significantly lower amounts of impurities were found on our electrodes (compare Figure 9), ASC values are comparable to values in Ref. 34 therefore this mechanism is very unlikely.

III) *Ni bulk as H reservoir:* For the Ni bulk as determining factor of the ASC, changes in hydrogen concentration were the likely capacitive mechanism. Dissolved hydrogen could diffuse from the bulk to the triple phase boundary, be oxidized there and desorb as water according to $2H_{Ni} + O_O^x \rightarrow H_2O + V_O^{\cdot\cdot} + 2e'_{Ni}$. (Mechanisms with hydrogen oxidation at the entire Ni/YSZ interface are discussed below.) In order to act purely capacitive, hydrogen concentration changes in the Ni bulk have to be accompanied by a fast reaction at the triple phase boundary. This is in contradiction to the rate limiting reaction at the triple phase boundary assumed for the resistances of Ni/YSZ electrodes.[11,30] Hence, this mechanism appears very unlikely.

IV) *Protons at the interface:* Another possible mechanism (also mentioned in Ref. 33) is based on the H/H$^+$ redox reaction $H_{Ni} + O_O^x \rightleftarrows OH_O^{\cdot} + e'_{Ni}$. Since protons are hardly soluble in the bulk of YSZ grains,[48] it is very likely that they can only be stored very close to the surface of a YSZ single crystal, i.e. in an interlayer between Ni and YSZ. For electroneutral incorporation of protons into this layer without drastic change of the electron concentration, also the oxygen vacancy concentration in this interface layer has to change. Actually, the proton concentration change can be considered as a consequence of the water activity variation at the interface and is determined by the defect equation $H_2O + V_O^{\cdot\cdot} + O_O^x \rightleftarrows 2OH_O^{\cdot}$. The water activity varies since the oxygen activity in YSZ varies by the voltage while the hydrogen content in Ni is fixed by the atmosphere. According to Equation 3 the minority charge carrier concentration in a 1 nm thick layer would have to be $1.7 \cdot 10^{21}\ cm^{-3}$ to explain an ASC of 3 F/m^2, which corresponds to ∼3 mol% with respect to oxygen sites in bulk YSZ. Since this is already close to the oxygen vacancy concentration, c_i in Equation 3 should be replaced by $c_{OH^{\cdot}} \cdot 4c_{V_O^{\cdot\cdot}}/(c_{OH^{\cdot}} + 4c_{V_O^{\cdot\cdot}})$,[46] but still realistic concentration values result.

The effect of sulfur exposure on the electrode capacitance could be explained by S at the Ni/YSZ interface stabilizing or occupying oxygen vacancies and thereby hindering the dissolution of protons in the YSZ as $OH_O^{\cdot}$. This mechanism is thus a second viable candidate to explain the absolute values of the ASC found here; the effect of the voltage would depend on the other charge carrier ($V_O^{\cdot\cdot}$ or $OH_O^{\cdot}$).

V) *Local oxidation of Ni:* This mechanism involves the formation of interfacial nickel oxide $Ni_{1-x}O$ with unknown Ni content. In principle, variation of the Ni stoichiometry in $Ni_{1-x}O$ can lead to a chemical capacitance as does oxygen variation in mechanism I. Owing to the absence of a Ni ion conducting electrolyte, however, oxide ions have to be involved in any defect chemical change of an interfacial $Ni_{1-x}O$ layer, i.e. formation of additional $Ni_{(1-x+y)/2}O$ is required:

$$yNi + Ni_{1-x}O + O_O^x \leftrightharpoons 2Ni_{(1-x+y)/2}O + V_{O,YSZ}^{\cdot\cdot} + 2e'_{Ni}$$

Bulk nickel oxide decomposes below a p_{O_2} of $\sim 10^{-14}$ bar at 800°C[49] and thus should not be present. Interfacial $Ni_{1-x}O$, however, might be stable also in the p_{O_2} regime considered here and may change its stoichiometry and Ni chemical potential by forming additional $Ni_{(1-x+y)/2}O$ according to the reaction shown above. Since rather large deviations of x,y from 1 might be involved, large chemical capacitances are easily conceivable. The interfacial layer visible in Figure 9 could be such a $Ni_{1-x}O$ layer. A similar capacitive mechanism has previously been suggested for Pt/YSZ electrodes in air.[50–52] Sulfur at the interface may affect the formation of such a $Ni_{1-x}O$ layer and can thus influence the capacitance. At some low p_{O_2} also interfacial $Ni_{1-x}O$ is expected to decompose and this kind of chemical capacitance should disappear at sufficiently negative voltages. This mechanism may therefore govern the bias range representing higher p_{O_2} values. The need for severe structural changes in this reaction may also explain the observed hysteresis in this range of Figure 7. Henceforth, this model is a very realistic candidate for explaining the capacitive behavior at polarizations above the equilibrium oxygen partial pressure of $7 \cdot 10^{-24}$ bar. For lower pressures either mechanism I or IV are considered to be most realistic.

Conclusions

In this study geometrically well-defined thin film electrodes with nominally equal circumferences and varying areas were prepared. Electrochemical impedance spectroscopy measurements at 800°C in H_2/H_2O atmosphere revealed a single depressed and slightly asymmetric semicircle in the Nyquist plot. Electrode capacitance values were obtained from impedance data via a CNLS-fit and effects of electrode size, electrochemical polarization, temperature and H_2S in the feed gas on the capacitance were analyzed.

In terms of possible capacitance forming mechanisms, a Helmholtz-type double layer, space charge models and various forms of chemical capacitance were discussed. Measurements on electrodes with different areas revealed an area specific capacitance of 3.01 ± 0.033 F/m^2, which is too high to be explained by a Helmholtz-type double layer. Additionally, since ion approach to the metal is limited (Stern model), a diffuse space charge layer cannot explain the ASC value either.

Therefore, contributions of chemical capacitances are the most likely cause of large parts of the capacitive behavior of the Ni/YSZ system. This interpretation is also backed by the dependence of the capacitance on the H_2S content of the measurement atmosphere. Ni surface modification by YSZ coverage did not lead to a significant reduction in capacitance, which indicates that the Ni surface does not play a key role in the mechanism of electrode capacitance formation. Also, a Ni bulk based capacitance could be excluded and only mechanisms at the Ni/YSZ interface are viable candidates to explain the capacitive behavior of Ni/YSZ electrodes.

The available data suggest two different capacitive mechanisms. One of them is dominating above an equilibrium oxygen partial pressure of $7 \cdot 10^{-24}$ bar and is characterized by a kind of hysteresis. In this p_{O_2} regime a mechanism involving oxidation of Ni and modification of an interfacial $Ni_{1-x}O$ layer is suggested to explain this capacitance.

For equilibrium oxygen partial pressures below $7 \cdot 10^{-24}$ bar, non-stoichiometry of YSZ or the H/H^+ redox pair with protons stored at the interlayer between Ni and YSZ bulk may cause the electrode capacitance.

Acknowledgment

The financial support by the Austrian Federal Ministry of Science, Research and Economy and the National Foundation for Research, Technology and Development is gratefully acknowledged.

The authors also acknowledge the TU Wien University Library for financial support through its Open Access Funding Program.

Further, the authors thank Dr. R. Iskandar from the Gemeinschaftslabor für Elektronenmikroskopie (RWTH Aachen) for performing the HR-TEM measurements.

References

1. A. B. Stambouli and E. Traversa, *Renewable and Sustainable Energy Reviews*, **6**, 433 (2002).
2. S. B. Adler, *Chemical Reviews*, **104**, 4791 (2004).
3. U. Anselmi-Tamburini, G. Chiodelli, M. Arimondi, F. Maglia, G. Spinolo, and Z. A. Munir, *Solid State Ionics*, **110**, 35 (1998).
4. S. P. Jiang and Y. Ramprakash, *Solid State Ionics*, **122**, 211 (1999).
5. H. Koide, Y. Someya, T. Yoshida, and T. Maruyama, *Solid State Ionics*, **132**, 253 (2000).
6. T. Fukui, K. Murata, S. Ohara, H. Abe, M. Naito, and K. Nogi, *Journal of Power Sources*, **125**, 17 (2004).
7. J. R. Wilson, W. Kobsiriphat, R. Mendoza, H.-Y. Chen, J. M. Hiller, D. J. Miller, K. Thornton, P. W. Voorhees, S. B. Adler, and S. A. Barnett, *Nat Mater.*, **5**, 541 (2006).
8. A. Hauch, S. H. Jensen, J. B. Bilde-Sørensen, and M. Mogensen, *Journal of The Electrochemical Society*, **154**, A619 (2007).
9. J. Mizusaki, H. Tagawa, T. Saito, T. Yamamura, K. Kamitani, K. Hirano, S. Ehara, T. Takagi, T. Hikita, M. Ippommatsu, S. Nakagawa, and K. Hashimoto, *Solid State Ionics*, **70–71**, Part 1, 52 (1994).
10. A. Bieberle and L. J. Gauckler, *Solid State Ionics*, **135**, 337 (2000).
11. A. Bieberle, L. P. Meier, and L. J. Gauckler *Journal of The Electrochemical Society*, **148**, A646 (2001).
12. D. Kek, M. Mogensen, and S. Pejovnik, *Journal of The Electrochemical Society*, **148**, A878 (2001).
13. K. Vels Jensen, S. Primdahl, I. Chorkendorff, and M. Mogensen, *Solid State Ionics*, **144**, 197 (2001).
14. A. Bieberle and L. J. Gauckler, *Solid State Ionics*, **146**, 23 (2002).
15. K. V. Jensen, R. Wallenberg, I. Chorkendorff, and M. Mogensen, *Solid State Ionics*, **160**, 27 (2003).
16. K. Norrman, K. V. Hansen, and M. Mogensen, *Journal of the European Ceramic Society*, **26**, 967 (2006).
17. A. M. Sukeshini, B. Habibzadeh, B. P. Becker, C. A. Stoltz, B. W. Eichhorn, and G. S. Jackson, *Journal of The Electrochemical Society*, **153**, A705 (2006).
18. M. Vogler, A. Bieberle-Hütter, L. Gauckler, J. Warnatz, and W. G. Bessler, *Journal of The Electrochemical Society*, **156**, B663 (2009).
19. W. G. Bessler, M. Vogler, H. Stormer, D. Gerthsen, A. Utz, A. Weber, and E. Ivers-Tiffee, *Physical Chemistry Chemical Physics*, **12**, 13888 (2010).
20. A. Ehn, J. Høgh, M. Graczyk, K. Norrman, L. Montelius, M. Linne, and M. Mogensen, *Journal of The Electrochemical Society*, **157**, B1588 (2010).
21. A. Utz, H. Störmer, A. Leonide, A. Weber, and E. Ivers-Tiffée, *Journal of The Electrochemical Society*, **157**, B920 (2010).
22. A. Utz, K. V. Hansen, K. Norrman, E. Ivers-Tiffée, and M. Mogensen, *Solid State Ionics*, **183**, 60 (2011).
23. A. Utz, J. Joos, A. Weber, and E. Ivers-Tiffée, *ECS Transactions*, **35**, 1669 (2011).
24. A. Weber, A. Utz, J. Joos, E. Ivers-Tiffée, H. Störmer, D. Gerthsen, V. Yurkiv, H.-R. Volpp, and W. G. Bessler, *ECS Transactions*, **35**, 1513 (2011).
25. Y. Shi, N. Cai, and Z. Mao, *International Journal of Hydrogen Energy*, **37**, 1037 (2012).
26. W. Yao and E. Croiset, *Journal of Power Sources*, **226**, 162 (2013).
27. W. Yao and E. Croiset, *Journal of Power Sources*, **248**, 777 (2014).
28. M. C. Doppler, J. Fleig, and A. K. Opitz, *ECS Transactions*, **68**, 1383 (2015).
29. W. Li, Y. Shi, Y. Luo, Y. Wang, and N. Cai, *Journal of Power Sources*, **276**, 26 (2015).
30. W. Yao and E. Croiset, *The Canadian Journal of Chemical Engineering*, **93**, 2157 (2015).
31. J. Fleig, F. S. Baumann, V. Brichzin, H. R. Kim, J. Jamnik, G. Cristiani, H. U. Habermeier, and J. Maier, *Fuel Cells*, **6**, 284 (2006).
32. A. K. Opitz, M. Kubicek, S. Huber, T. Huber, G. Holzlechner, H. Hutter, and J. Fleig, *Journal of Materials Research*, **28**, 2085 (2013).
33. S. Primdahl and M. Mogensen, *Journal of The Electrochemical Society*, **144**, 3409 (1997).
34. K. V. Hansen, K. Norrman, and M. Mogensen, *Journal of The Electrochemical Society*, **151**, A1436 (2004).
35. M. G. H. M. Hendriks, J. E. ten Elshof, H. J. M. Bouwmeester, and H. Verweij, *Solid State Ionics*, **146**, 211 (2002).
36. F. S. Baumann, J. Fleig, H.-U. Habermeier, and J. Maier, *Solid State Ionics*, **177**, 1071 (2006).
37. C. H. Hsu and F. Mansfeld, *Corrosion*, **57**, 747 (2001).
38. M. de Ridder, R. G. van Welzenis, A. W. D. van der Gon, H. H. Brongersma, S. Wulff, W.-F. Chu, and W. Weppner, *Journal of Applied Physics*, **92**, 3056 (2002).
39. M. de Ridder, R. G. van Welzenis, H. H. Brongersma, and U. Kreissig, *Solid State Ionics*, **158**, 67 (2003).
40. M. de Ridder, A. G. J. Vervoort, R. G. van Welzenis, and H. H. Brongersma, *Solid State Ionics*, **156**, 255 (2003).
41. J. O. M. Bockris, A. K. N. Reddy, and M. Gamboa-Aldeco, *Modern Electrochemistry 2A: Fundamentals of Electrodics*, Springer, US (2000).
42. M. Gong, X. Liu, J. Trembly, and C. Johnson, *Journal of Power Sources*, **168**, 289 (2007).
43. R. J. Brigham, H. Neumayer, and J. S. Kirkaldy, *Canadian Metallurgical Quarterly*, **9**, 525 (1970).
44. S. Floreen and J. H. Westbrook, *Acta Metallurgica*, **17**, 1175 (1969).
45. G. L. Kellogg, *The Journal of Chemical Physics*, **83**, 852 (1985).
46. J. Jamnik and J. Maier, *Physical Chemistry Chemical Physics*, **3**, 1668 (2001).
47. J. H. Park and R. N. Blumenthal, *Journal of The Electrochemical Society*, **136**, 2867 (1989).
48. N. Sakai, K. Yamaji, T. Horita, H. Kishimoto, Y. P. Xiong, and H. Yokokawa, *Solid State Ionics*, **175**, 387 (2004).
49. H. Yokokawa, H. Kishimoto, K. Yamaji, and T. Horita, *ECS Transactions*, **25**, 2131 (2009).
50. G. Fóti, A. Jaccoud, C. Falgairette, and C. Comninellis, *J Electroceram*, **23**, 175 (2009).
51. A. Jaccoud, C. Falgairette, G. Fóti, and C. Comninellis, *Electrochimica Acta*, **52**, 7927 (2007).
52. A. K. Opitz and J. Fleig, *Solid State Ionics*, **181**, 684 (2010).